CHEMISTRY OF MATERIALS

Open Access

pubs.acs.org/cm

Article

Multifunctional Polypeptide-Based Nanoconjugates for Targeted Mitochondrial Delivery and Nonviral Gene Therapy

Published as part of Chemistry of Materials special issue "Polymer-Drug Conjugate Materials".

Camilla Pegoraro, Esther Masiá Sanchis, Snežana Đorđević, Irene Dolz-Pérez, Cristián Huck-Iriart, Lidia Herrera, Sergio Esteban-Pérez, Inmaculada Conejos-Sanchez,* and María J. Vicent*

Cite This: *Chem. Mater.* 2025, 37, 1457−1467

Read Online

ACCESS | Metrics & More | Article Recommendations | Supporting Information

ABSTRACT: Despite recent advances in nanomedicine, developing multifunctional nanocarriers capable of targeted subcellular delivery and efficient gene therapy remains a significant challenge. This study reports the design, synthesis, and evaluation of a novel multifunctional polypeptide-based nanoconjugate that addresses this gap using sequential delivery, combining mitochondrial targeting and nonviral gene therapy. We engineered a poly-L-ornithine-based, polyethylene glycol-modified carrier and introduced a novel custom-designed trivalent compound (TRV3) into the structure. TRV3, conjugated to the polypeptide carrier via a redox-sensitive disulfide linker, incorporates the well-described triphenylphosphonium moiety (TPP) for mitochondrial targeting and a Cy5 fluorophore as a model drug. The resulting nanoconjugate (C-TRV3-A) demonstrated efficient endosomal escape and mitochondrial localization. Leveraging the endosomolytic properties of C-TRV3-A, we explored its potential as a nonviral vector for gene therapy. After optimizing formulation stability using a VLC-3 anionic polypeptide coating, we developed plasmid DNA polyplexes that exhibited enhanced stability and transfection efficiency in basic and advanced triple-negative breast cancer cell culture models. This multifunctional polypeptide-based nanoconjugate represents a significant advance in the field, offering a chemically versatile platform for simultaneous subcellular targeting and gene delivery that may be used in targeted cancer treatments, among other pathologies.

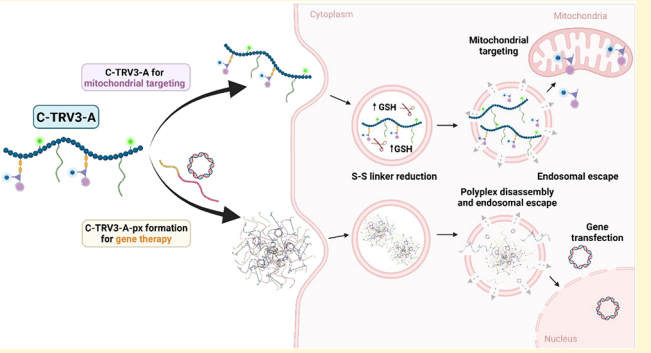

1. INTRODUCTION

Nanomedicine engineering presents a promising approach to enhance therapeutic outcomes in complex, multifactorial disorders such as cancer.[1] The rational design of multifunctional polymeric carriers and nanoconjugates with tailored properties enables the implementation of versatile/combination therapies, potentially improving efficacy and safety.[2,3] Biodegradable polypeptides lacking immunogenicity offer advantages when used as polymeric carriers, including tunable properties (via controlled synthesis, architecture, and post-polymerization modification) and the multivalency required for the conjugation of distinct payloads via bioresponsive linkers.[4,5] Integrating the described features will support the creation of polypeptide-based nanoconjugates with diverse functionalities.[6]

Numerous applications, including clinically tested,[7] have demonstrated polypeptide versatility,[8,9] while their potential for targeting specific subcellular compartments/delivering genetic payloads has been independently studied.[10−13] However, combining these two functionalities within a single polypeptide-based system remains mostly unexplored. Of note, mitochondria have emerged as a primary focus of subcellular targeting efforts due to their critical role in energy generation and cancer cell survival.[14]

Here, we designed a versatile multifunctional polypeptide-based nanoconjugate for mitochondrial targeting following a rational hierarchical delivery approach. We selected poly-L-ornithine (PLO) as the polymeric carrier due to its endosomal escape properties.[10,15] To enhance functionality, we modified PLO with a polyethylene glycol chain (PLO−PEG), which improves steric stability and minimizes nonspecific interactions.[16] Our group's prior research underscored the critical role of PEG modification and the significance of molecular weight (Mw).[17] Among various derivatives evaluated, PLO−PEG_{3000} - used as the starting carrier in this study -

Received: October 1, 2024
Revised: January 9, 2025
Accepted: January 10, 2025
Published: February 5, 2025

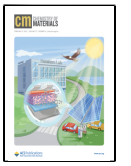

demonstrated optimal transfection efficiency compared to alternatives such as PLO−PEG_{2000}. We conjugated a trivalent compound (TRV3), incorporating a triphenylphosphonium (TPP) derivative for mitochondrial targeting[18,19] and Cy5 as a model drug, to PLO−PEG via a redox-sensitive disulfide (S−S) linker[20] (C-TRV3). Finally, we labeled the nanoconjugate with Atto488 at ornithine pendant groups for tracking purposes (C-TRV3-A). Overall, we observed effective TRV3 release following S−S linker reduction and endosomal escape, enabling mitochondrial targeting. The endosomolytic properties of C-TRV3-A supported subcellular targeting and applications in gene therapy as a nonviral vector. While polycationic polymers such as PLO support DNA condensation and cellular uptake,[17,21−24] their toxicity can limit gene therapy applications.[25−27] We employed a polyanionic polypeptide (VLC-3)[28] as an anionic coating to improve polyplex stability and safety to address this limitation. We formulated plasmid (p)DNA polyplexes using C-TRV3-A and VLC-3, optimizing them for high stability and transfection efficiency in the triple-negative breast cancer (TNBC) MDA-MB-231 cell model.

This study explores the innovative use of polypeptide-based nanoconjugates for targeted mitochondrial delivery, paving the way for enhanced therapeutic strategies in cancer treatment and improved safety profiles in nonviral gene therapy applications.

2. EXPERIMENTAL SECTION

Details regarding materials, protocols, and conditions for the synthesis and biological evaluation of C-TRV3-A and polyplexes are extensively described in the ESI and summarized in the following sections.

2.1. Materials. PLO (5700 g mol^{-1}, n = 50) was provided by Curapath (Valencia, Spain). The heterobifunctional PEG-derivative MeO-PEG_{3000}-NHS (3023 g/mol; NHS = *N*-hydroxysuccinimide and MeO = methoxy) was purchased from Biopharma PEG (USA). N*β*-Fmoc-N*ω*-Boc-L-*β*-homolysine and 3,3′-dithiopropionic acid di(N-succinimidyl ester (S−S linker derivative) were purchased from ABCR GmbH (Germany). (3-carboxypropyl)triphenylphosphonium bromide (TPP derivative, CTPB) was purchased from Sigma-Aldrich (USA). The fluorophores $Atto_{488}$-NHS and Cyanine5-amine (Cy5-NH_2) were purchased from ATTO-TEC GmbH and Lumiprobe GmbH (Germany). Plasmid pCMV-Luc (pDNA-Luc, Luc = luciferase) was purchased from Plasmid Factory (Germany).

2.2. Methods. *2.2.1. Synthesis and Characterization of C-TRV3-A. 2.2.1.1. Synthesis of C-TRV-3-A.* Briefly, N*β*-Fmoc-N*ω*-Boc-L-*β*-homolysine (S1, 35.4 mg, 1.20 eq., 5 mg/mL) was dissolved in anhydrous dimethylformamide (DMF) in a two-neck flask in an N_2 atmosphere. 4-(4,6-dimethoxy-1,3,5-triazin-2-yl)-4-methylmorpholinium tetrafluoroborate (DMTMM BF4) (48.2 mg, 2.40 equiv) in 0.5 mL anhydrous DMF was added to activate the carboxylic groups (20 min, room temperature). Cy5-NH_2 (40 mg, 1 eq., 10 mg/mL) in anhydrous DMF was added, and the pH was adjusted to 8 with N, N-diisopropylethylamine. The reaction proceeded for 24 h at room temperature, protected from light. After solvent removal, the product (S2, theoretical yield: 68.4 mg) underwent Boc-deprotection using dichloromethane (DCM)/trifluoroacetic acid (TFA) (2:1 v/v) for 2 h at room temperature. The final product (S3) was precipitated in cold diethyl ether, centrifuged, and lyophilized (Yield: 85%, 58.1 mg).

CTPB (31.6 mg, 1.20 eq., 4 mg/mL) in DMF was activated with DMTMM BF4 (48.3 mg, 2.4 equiv) for 20 min and then added to a solution of S3 (58.1 mg, 1 eq., 7 mg/mL) in anhydrous DMF. The pH was adjusted to 8 and reacted for 24 h at room temperature. The product (S4, theoretical yield: 83.4 mg) was precipitated, centrifuged, and lyophilized. S4 underwent Fmoc-deprotection in DMF/piperidine (4:1 v/v) for 4.5 h, and the final product (S5) was isolated by precipitation (Yield: 78%, 65 mg).

A solution of S5 (65 mg, 1.00 eq, 7 mg/mL) in anhydrous DMF was reacted with the S−S linker derivative (50.1 mg, 2 eq., 5 mg/mL) and a catalytic amount of 4-dimethylaminopyridine (DMAP) at pH 8 for 24 h. The product (TRV3) was purified by solid-phase extraction using silica cartridges with a DCM/methanol gradient (Yield: 70%, 57.9 mg).

PLO (S6, 200 mg, 1 eq., 20 mg/mL) in anhydrous dimethyl sulfoxide (DMSO) was reacted with MeO-PEG_{3000}-NHS (i.e., 123 mg, 0.04 eq. for a 4% mol PEG modification) and a catalytic amount of DMAP at pH 8 for 72 h. The product (S7) was purified by size exclusion chromatography (PD-10 columns) (PEG functionalization: 3.6% mol).

TRV3 (i.e., 53.7 mg, 0.10 eq for 10% mol PEG modification) was conjugated to S7 (100 mg, 1 eq., 4 mg/mL), forming C-TRV3 and purified by size exclusion chromatography (PD-10 columns) and ultrafiltration (Vivaspin, 2000 MWCO) (C-TRV3 functionalization: 4% mol; Cy5 loading: < 1 wt %; conjugation efficiency: 40%).

C-TRV3 (1 eq., 10 mg/mL) was labeled in water with Atto488-NHS (0.010 eq., 1.0% mol) in DMSO at pH 8 overnight. The product (C-TRV3-A) was purified by size exclusion chromatography (PD-10 columns) (conjugation efficiency: 90−100%).

Reported yields calculated based on the limiting reagent in each reaction. The functionalization/conjugation efficiencies of S7, C-TRV3, and C-TRV3-A were calculated by ^{1}H NMR or fluorescence spectroscopy.

2.2.1.2. C-TRV3-A Physicochemical Characterization. Structural characterization was performed using ^{1}H NMR spectroscopy (300 MHz Bruker spectrometer in $CDCl_3$ or D_2O). Mass spectrometry (MS) analysis employed direct injection Q1 scans (20 *μ*L, 50% acetonitrile/50% H_2O with 0.1% formic acid). The mass spectra presented in the ESI are centroid *m*/*z* values and background-subtracted spectra. To note, the mass of product S4 was identified as 1273.4 *m*/*z* and attributed to the decomposition of triphenylphosphine under electron impact, which results in the loss of one phenyl group and the formation of a two-charged ion (637.2 *m*/*z*). This behavior was limited in subsequent steps by reducing the ionization temperature from 750 to 250 °C and the declustering potential to 40 V. Moreover, Dynamic light scattering (DLS) measurements were conducted using a Malvern Zetasizer NanoZS instrument in phosphate-buffered saline (PBS) at 25 °C. Transmission electron microscopy (TEM) imaging was conducted on an FEI Tecnai Spirit BioTwin microscope with samples negatively stained using 2% uranyl acetate. Small-angle X-ray scattering (SAXS) experiments were performed at the NCD-SWEET beamline (ALBA Synchrotron, Barcelona, Spain) using X-ray energies of 12.4 and 15 keV, with data analyzed using a fractal coil model.

2.3. Synthesis of the Noncovalent Shielding Polyanion PSar-*b*-PGA Block Copolymer (VLC-3). The synthesis and full characterization of the block copolymer $PSar_{100}$-*b*-PGA_{15}OtBu (VLC-3) was conducted as described in the patent application ref. WO2023002014A1[28] and can be found in the ESI. Briefly, Sarcosine N-carboxyanhydride (Sar NCA) was polymerized in an anhydrous DMF solution under an inert atmosphere with *n*-butylamine as the initiator. The reaction proceeded at 10 °C overnight. Upon completion, the reaction mixture became clear and full conversion of the monomer could be detected by IR. Subsequently, Glutamic acid t-*tert*-butyl ester NCA, dissolved in anhydrous DMF, was introduced into the reaction mixture and stirred under the same conditions overnight. The resulting product was precipitated in diethyl ether, isolated by centrifugation, and dried under vacuum to yield the block copolymer as a white solid. Yield: 70−90%.

Next, the block copolymer of $PSar_{100}$-*b*-PGA_{15}OtBu was dissolved in trifluoroacetic acid at 0 °C, and the mixture was stirred at 5 °C for 1 h. The reaction mixture was then precipitated in diethyl ether, and the product was collected by centrifugation and dried under vacuum. The deprotected block copolymer was isolated as a white solid. Yield: 95%. The product was characterized by size exclusion chromatography Mw 9.2 kDa (Mw Salt), PDI: 1.09

2.4. C-TRV3-A Biological Characterization. *2.4.1. Cell Viability Assay.* MDA-MB-231 cells were seeded in 96-well plates (5,000 cells/

https://doi.org/10.1021/acs.chemmater.4c02742
Chem. Mater. 2025, 37, 1457−1467

Scheme 1. Complete Synthetic Procedure for C-TRV3-A Preparation[a]

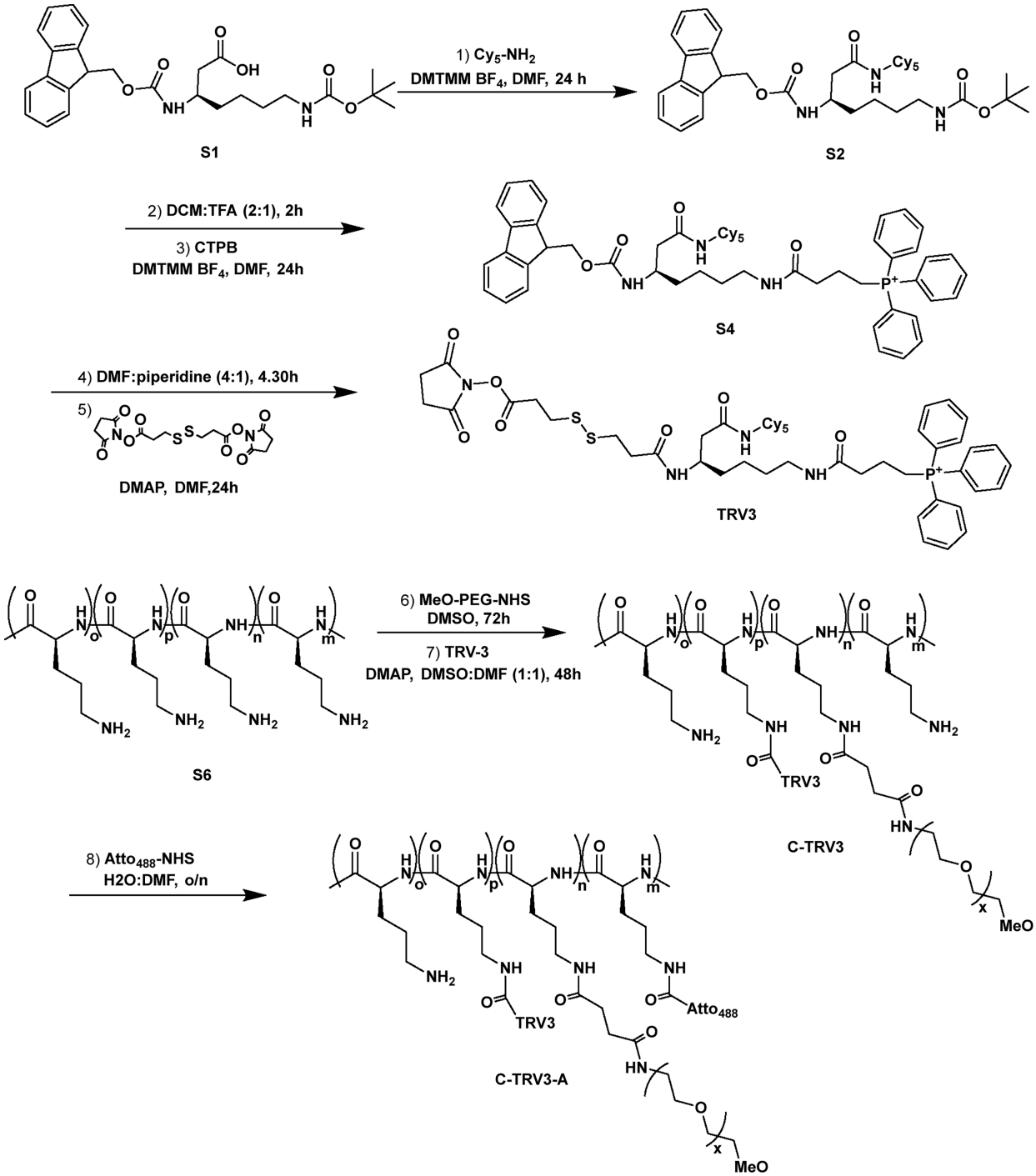

[a]S1: Nβ-Fmoc-Nω-Boc-L-β-homolysine; S2: Lys-Cy5; S4: Lys-Cy5-TPP; TRV3: Lys-Cy5-TPP−S-S; S6: PLO; C-TRV3: PLO−PEG conjugated to C-TRV3; C-TRV3-A: C-TRV3 conjugated to Atto488.

well) and incubated for 24 h at 37° and 5% CO_2. C-TRV3-A was added at a 0−1 mg/mL concentration range. Cell viability was assessed using the MTS/PMS assay after 72 h of incubation, with absorbance measured at 490 nm.

2.4.2. Cellular Uptake Studies. Confocal microscopy (Leica TCS SP8) was used to study the cellular uptake of C-TRV3-A in MDA-MB-231 cells. Cells were seeded in 384-well plates and incubated with nontoxic concentrations of C-TRV3-A. MitoTracker and LysoTracker were used to label mitochondria and lysosomes. Pulse-chase and time-lapse studies were conducted over various time points (1, 2, 4, 6 h for pulse-chase and every 20 s over 10 h for time-lapse studies). Images were processed using LAS X software and the ImageJ-JACoP plugin for colocalization analysis.

2.5. pDNAluc Polyplex Preparation and Characterization. *2.5.1. Polyplex Formation.* Polyplexes were prepared using pDNA-Luc (P, 200 ng), C-TRV3-A (N, cationic polymer), and VLC-3 (O, anionic shielding polymer $PSar_{100}$-*b*-PGA_{15}) at specified amine to phosphate (N/P) and oxygen to amine (O/N) ratios. Each component was diluted in separate tubes with Milli-Q water. N/P calculations considered only protonable nitrogens, excluding amide nitrogens, and accounted for PLO functionalization with PEG (3.6 mol %), TRV3 (4 mol %), and Atto488 (1 wt %). Complexation was

https://doi.org/10.1021/acs.chemmater.4c02742
Chem. Mater. 2025, 37, 1457−1467

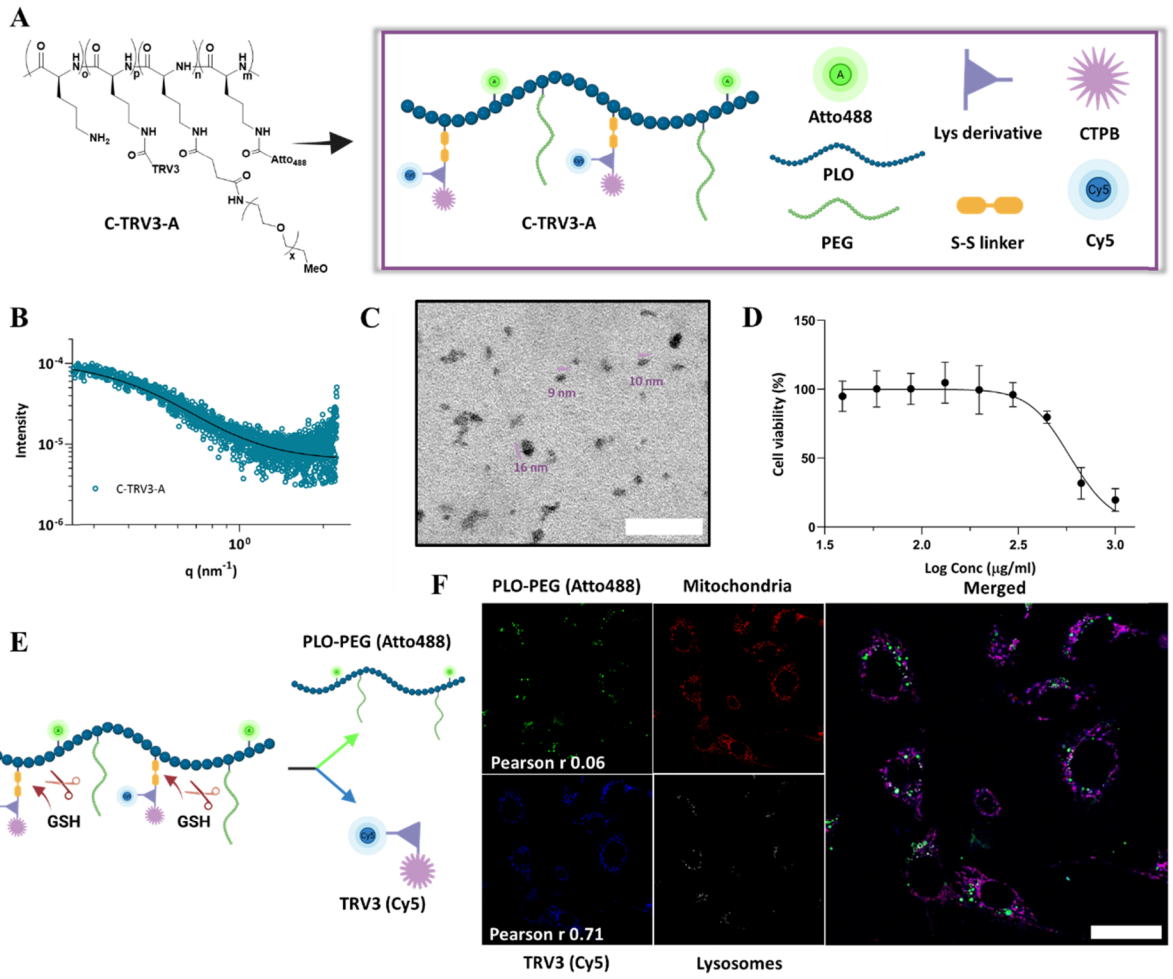

Figure 1. Physicochemical and biological characterization of C-TRV3-A. A) Chemical structure and schematic representation of C-TRV3-A. **B**) Small-angle X-ray scattering (SAXS) data for C-TRV3-A. Intensity expressed as a function of the scattering momentum transfer, q ($q = 4\pi\sin(\theta)/\lambda$). **C**) Transmission electron microscopy (TEM) image of C-TRV3-A, showing a size of 10−20 nm (diameter). Scale bar = 50 nm. **D**) MDA-MB-231 cell viability by MTS/PMS in response to C-TRV3-A exposure (IC_{50} = 0.5 mg/mL, 72 h, n = 3, mean ± SEM). **E**) TRV3 (bearing Cy5) release mechanism from C-TRV3-A in MDA-MB-231 cells. Schematic illustration showing TRV3 release from PLO−PEG (labeled with Atto488) after cytosolic delivery and S−S linker cleavage in a reductive environment. **F**) Confocal images of MDA-MB-231 cells 4 h post-treatment. Lysosomes (white, LysoTracker Blue), mitochondria (red, MitoTracker Red CM-H2Xros), TRV3 (blue, Cy5), and PLO−PEG (green, Atto488) shown. Purple regions indicate TRV3-mitochondria colocalization. Pearson r values calculated using the ImageJ JACoP plugin. Scale bar: 10 μm.

achieved by mixing pDNA-Luc with VLC-3 followed by C-TRV3-A addition with vigorous pipetting and a 20 min incubation at room temperature. Size distribution was determined by DLS, and electrophoresis assays were conducted to ensure polyplex formation.

2.5.2. Polyplex Interaction and Stability Assays. Interactions between pDNAluc, VLC-3, and C-TRV3-A and polyplex stability were evaluated using complementary assays. Heparin displacement assays were conducted by incubating polyplexes with 0.75 and 50 UI/ml heparin and analyzing nucleic acid release via gel electrophoresis and ultraviolet illumination. Plasma stability was assessed by incubating polyplexes in 20% mouse or human serum at 37 °C for 1 h, followed by gel electrophoresis. Stability in cell culture media was examined by incubating polyplexes in 80% DMEM/F-12 medium (10% fetal bovine serum (FBS)/1% penicillin-streptomycin (P/S)) at 37 °C for 1 h before gel electrophoresis analysis.

2.5.3. Polyplex Hemocompatibility Assay. Mouse red blood cells were isolated from fresh blood collected via cardiac puncture. Blood was diluted with phosphate-buffered saline (PBS; pH 7.4) and then centrifuged at 3000 rpm for 10 min at 4 °C three times. The final red blood cell pellet was resuspended to 2% (v/v) in sterile PBS. C-TRV3-A and polyplex solutions were prepared in PBS (pH 7.4). Samples were evaluated in triplicate at concentrations of 0.08, 0.04, and 0.01 mg/mL; PBS and 1% (w/v) Triton X-100 served as negative control. After a 1-h incubation at 37 °C, plates were centrifuged (3000 rpm, 10 min, room temperature). Supernatants were analyzed for hemoglobin release by measuring absorbance at 570 nm. The hemolysis percentage was calculated relative to Triton X-100-induced complete lysis.

2.5.4. Polyplex Biological Characterization. 2.5.4.1. Cell Viability in 2D and 3D In Vitro Cell Models. MDA-MB-231 cells were used for 2D and 3D culture viability assays. For 2D cultures, cells were seeded in 96-well plates (5,000 cells/well) in DMEM (high glucose/no phenol red with 10% FBS/1% P/S) and incubated for 24 h. Polyplexes were prepared in PBS and added to wells after a 20 min incubation. Cell confluency was assessed at 24, 48, and 72 h using Hoechst 33342 staining, with fluorescence measured at 450 nm. For 3D cultures, cells were seeded in 96-well ultralow attachment plates (10,000 cells/well) using DMEM (high glucose/no phenol red) supplemented as described in the ESI. Polyplexes were added as in the 2D culture setup. After a 24-h incubation, cell viability was evaluated using an MTS/PMS assay, with absorbance measured at 490 nm. Polyethylenimine (JetPEI, referred to as PEI) (N/P = 1) and nonformulated pDNA-Luc served as positive and negative controls. Cell viability was expressed as a percentage relative to untreated controls, with values representing the mean ± SEM (n > 3).

https://doi.org/10.1021/acs.chemmater.4c02742
Chem. Mater. 2025, 37, 1457−1467

2.5.4.2. Transfection in 2D and 3D In Vitro Cell Models. MDA-MB-231 cells were used for both 2D and 3D luciferase expression assays. For 2D cultures, cells were seeded for 24 h in 96-well plates (5,000 cells/well) in DMEM (high glucose, no phenol red, 10% FBS, 1% P/S). For 3D cultures, cells were seeded for 24 h in ultralow attachment plates (10,000 cells/well) in DMEM supplemented as described in the **ESI**. Polyplexes were prepared in PBS and added to wells after a 20 min incubation. PEI-based polyplexes were prepared according to the manufacturer's guidelines. Luciferase activity was measured using Bright-Glo reagent by EnSight Multimode Plate Reader (535 nm) after 24 h (3D) or 24, 48, and 72 h (2D) of incubation. Luminescence values were normalized to cell viability and background subtracted. PEI (N/P = 1) and nonformulated pDNA-Luc served as positive and negative controls. Results are expressed as the mean ± SEM ($n > 3$).

3. RESULTS AND DISCUSSION

3.1. C-TRV3-A Synthesis and Characterization. We synthesized nanoconjugate C-TRV3-A using a controlled eight-step procedure (Scheme 1), which involved trivalent compound TRV3 synthesis and conjugation to the polymeric carrier (**ESI**), with each intermediate characterized via ^{1}H NMR and MS.

The initial coupling of Nβ-Fmoc-Nω-Boc-L-β-homolysine (Lys derivative, S1) with Cy5-NH_2 in anhydrous DMF yielded Lys-Cy5 (S2) (Scheme S1), which we confirmed by characteristic ^{1}H NMR signals (Figure S1) and MS fragmentation patterns (Figure S2). Subsequent Boc deprotection of S2 using a DCM/TFA mixture produced S3 (85% yield) (Scheme S2; Figures S3 and S4). We then efficiently conjugated CTPB (TPP derivative) to S3, forming Lys-Cy5-TPP (S4) (Scheme S3; Figures S5 and S6). Fmoc deprotection of S4 used a 4:1 mixture of DMF and piperidine (78% yield) (Scheme S4; Figures S7 and 8). A critical step involved introducing the S−S linker to S5 using 3,3′-dithiopropionic acid di(N-succinimidyl ester) to form TRV3 (Scheme S5; Figures S9 and S10). In parallel, we conjugated MeO-PEG_{3000}-NHS to PLO (Scheme S6), with PEG functionalization quantified at 3.6 mol % (Figure S11).

The synthesis proceeded with TRV3 conjugation to PLO−PEG (S7) (Scheme S7), yielding C-TRV3 (C = nano-Conjugate) with 4 mol % TRV3 functionalization (Figure S12). We observed Cy5 loading, determined by fluorescence spectroscopy, at less than 1 mol % (Figure S13). Finally, we labeled C-TRV3 with Atto488-NHS (A) to form C-TRV3-A (Scheme S8) at 90−100% conjugation efficiency and % wt modification (Figure S14). The careful control of reaction conditions and thorough purification methods throughout synthesis ensured product quality.

The comprehensive characterization of all intermediates and the final nanoconjugate by ^{1}H NMR, MS, and fluorescence spectroscopy ensured the integrity and functionality of the final nanoconjugate C-TRV3-A (Figure 1A). Zeta potential measurements revealed a positively charged compound (7.68 ± 0.03 mV), suggesting that TRV3, Atto488, and PEG functionalization did not fully mask the cationic nature of PLO and that C-TRV3-A retains potential for electrostatic interactions with negatively charged compounds[29] or cellular membranes.[30] The SAXS pattern for C-TRV3-A exhibited a slope of approximately −3 in the Porod region (in log−log scale)[31] (Figure 1B), indicating a structure with a dense core. Although initially developed for linear polymer systems, we utilized the fractal coil model as a general framework for estimating polymer size; the lack of significant changes in polymer structural features upon labeling with Atto488 justified this approach. We found a radius of gyration (Rg) of C-TRV3-A, calculated using the fractal coil model, of 3.60 ± 0.05 nm. Transmission electron microscopy (TEM) imaging corroborated SAXS results, revealing an average nanoconjugate diameter of 5−15 nm (Figure 1C). The slight variation between SAXS and TEM measurements can be attributed to the irregular shapes and polydispersity observed in TEM images, in contrast to the mathematical model applied to the entire SAXS data set, which assumes a more uniform particle distribution.[32] Even though there is no discrepancy between the measurements, and they fall within the same range, these methodological differences account for the minor variations observed.

The multistep synthesis and thorough characterization of C-TRV3-A provided a comprehensive understanding of its structural and physicochemical properties, establishing a robust basis for subsequent biological evaluations and potential therapeutic applications.

3.2. TRV3 Release from C-TRV3-A Supports Mitochondrial Targeting. Cell viability assays using MDA-MB-231 cells as a model demonstrated the moderate cytotoxic profile of C-TRV3-A after a 72-h exposure (IC_{50} = 0.5 mg/mL) (Figure 1D), which is likely attributable to C-TRV3-A's polycationic nature. After establishing a range of nontoxic concentrations, we investigated C-TRV3-A cell internalization and subcellular localization using live-cell confocal fluorescence microscopy in MDA-MB-231 cells at various time points (1, 2, 4, and 6 h; Figure S15 - pulse-chase study). C-TRV3-A comprises PLO, a biodegradable polycationic peptide with endosomal escape properties;[15] an S−S linker, reducible in endocytic compartments rich in glutathione (GSH) and the gamma-interferon-inducible lysosomal thiol reductase GILT[33] (especially in breast cancer[34]); and CTPB, a widely exploited mitochondrial targeting moiety[18,19] (Schematic illustration, Figure 1E). The dual-monitoring probe labeling strategy of C-TRV3-A (Cy5 conjugated to TRV3 and Atto488 conjugated to PLO−PEG) enabled the observation of TRV3 release via S−S linker cleavage in the reductive endosomal compartment, followed by endosomal escape and mitochondrial targeting. Quantitative image analysis using Pearson's correlation coefficient (Pearson r) revealed distinct intracellular localization patterns for TRV3 and PLO−PEG after a 4-h incubation (Figure 1F). TRV3 demonstrated significant colocalization with mitochondria (MitoTracker Red), as indicated by a Pearson r of 0.71, visualized as purple regions in Figure 1F. Meanwhile, PLO−PEG exhibited minimal mitochondrial colocalization (Pearson r = 0.06) and non-significant interactions with lysosomes (LysoTracker Blue), reflected by a Pearson r of 0.22, suggesting endosomal escape prior to lysosomal accumulation. These results suggest that PLO facilitated successful endosomal escape following endocytosis, while S−S linker reduction ensured TRV3 release, which CTPB subsequently targeted to the mitochondria. The successful visualization of the C-TRV3-A internalization pathway and subcellular targeting corroborated the rational design of the nanoconjugate.

Our results demonstrate the successful design and functionality of C-TRV3-A, confirming an ability to undergo cellular internalization, endosomal escape, and targeted mitochondrial delivery, thus validating its potential as a versatile nanocarrier for intracellular drug delivery.

https://doi.org/10.1021/acs.chemmater.4c02742
Chem. Mater. 2025, 37, 1457−1467

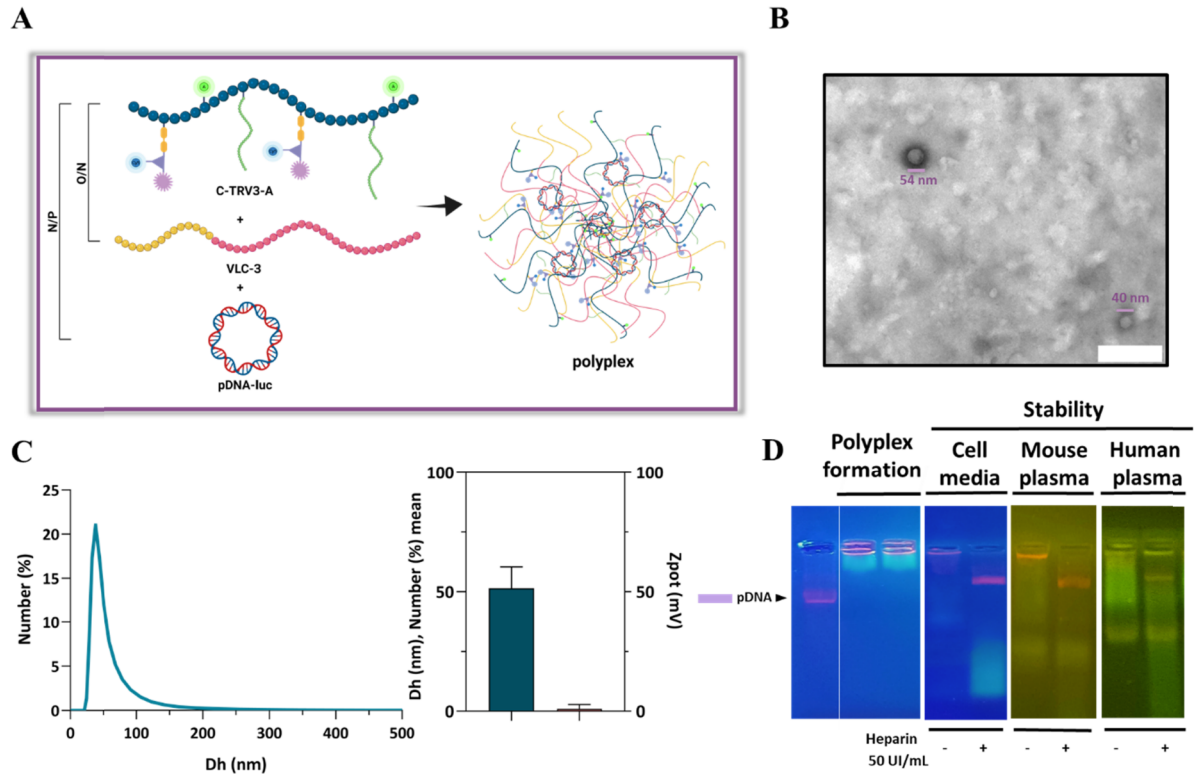

Figure 2. C-TRV3-A-based polyplex formation, physicochemical characterization, and stability. **A**) Schematic representation of C-TRV3-A-px formation using pDNA-Luc (P, 200 ng/mL), C-TRV3-A (N, cationic polymer), and VLC-3 (O, anionic shielding polymer) at specified amine to phosphate (N/P) and oxygen to amine (O/N) ratios. **B**) Transmission electron microscopy (TEM) image of Px02501 (O/*N* = 0.25, N/*P* = 1, in PBS at C-TRV3-A = 0.02 mg/mL) revealed a size of 40−70 nm (diameter). Scale bar = 100 nm. **C**) Left: Size distribution graph of Px02501 expressed as number of molecules (%) per hydrodynamic diameter (Dh) obtained by dynamic light scattering (DLS) in PBS at C-TRV3-A = 0.02 mg/mL. Right: Hydrodynamic diameter (Dh = 51 ± 9 nm) and zeta-potential (Zpot = 0.93 ± 1.8 mV) analysis of Px02501 determined by DLS. **D**) Shift-gel assays of Px02501 prepared using pDNA-Luc (P, 200 ng), C-TRV3-A (N, cationic polymer), and VLC-3 (O, anionic shielding polymer) in PBS and their stability in cell media (DMEM (high glucose/no phenol red with 10% FBS/1% P/S), mouse plasma, and human plasma. Polyplexes were incubated for 1 h at 37 °C before heparin addition. pDNA in purple, C-TRV3-A in green, and VLC-3 not visible under an ultraviolet lamp; therefore, an ultraviolet filter was applied to enhance gel visualization for mouse and human plasma.

3.3. Formulation and Characterization of C-TRV3-A-Based Polyplexes for Nonviral Gene Delivery. To harness the endosomolytic properties for nonviral gene delivery, we incorporated C-TRV3-A into polyplexes. Polycationic polymers have been widely explored for the formation of polyplexes based on electrostatic interactions between the polymer and negatively charged genetic payloads.[35] Specifically, PLO has been evaluated due to its biodegradability and ability to condense DNA and facilitate cellular uptake;[17,21−24] however, the relative toxicity of C-TRV3-A, as observed with many cationic polymers,[25−27] could limit applications in gene therapy. Approaches to mask PLO positive charges and reduce toxicity include polyplex functionalization with charge-conversion polymers[36] (anionic in the extracellular environment and cationic in the endolysosomal compartment), the guanidation of hyperbranched PLO-based polymers,[37] or the formulation of lipoplexes.[38]

We employed $PSar_{100}$-*b*-PGA_{15} diblock copolymer, a polyanionic polypeptide VLC-3,[28] as a polymeric coating to improve polyplex stability and safety (see **ESI**, Scheme S9, Figure S16). Previous examples exploiting the anionic mucopolysaccharide hyaluronic acid supported the application of this strategy,[39−41] increasing DNA/PEI polyplex safety while reducing nonspecific protein interaction and enhancing transcriptional activity. We formulated polyplexes (C-TRV3-A-px) using pDNA-Luc (P), C-TRV3-A (N, cationic polymer), and VLC-3 (O, anionic shielding polymer) at various O/N and N/P ratios (Figure 2A) in PBS and verified complexation by shift-gel assay (Figure S17). The Atto488 labeling included in the C-TRV3-A structure supported the enhanced visualization of C-TRV3-A-px components in gels and improved the interpretation of results. We identified an N/P ratio of 1 as optimal for the interaction between genetic material and polycationic polymer. Higher N/P ratios (1.25, 1.5, 5, 10, and 15) resulted in excess free C-TRV3-A, as evidenced by diffusion and smearing in the gel (Figure S17A), which could induce cytotoxicity. We evaluated the O/P at 0.25, 0.5, 1, and 2, with effective C-TRV3-A-px formation observed across all tested ratios (Figure S17B). Further characterization focused on C-TRV3-A-px with an O/P ratio of 0.25 (Px02501, N/P fixed at 1), demonstrating significantly higher in vitro transfection efficiency (detailed below). TEM and dynamic DLS analysis confirmed Px02501 formation, with TEM imaging revealing a diameter ranging from 40 to 70 nm (Figure 2B), consistent with DLS measurements that indicated an average diameter of 51 ± 9 nm (Figure 2C). Zeta potential analysis further corroborated Px02501 formation, yielding a value of 0.93 ± 1.8 mV (Figure 2C), which differed significantly from the 7.68 ± 0.03 mV previously measured for C-TRV3-A.

The successful formulation of C-TRV3-A-px with optimized N/P and O/P ratios and their physicochemical character-

https://doi.org/10.1021/acs.chemmater.4c02742
Chem. Mater. 2025, 37, 1457−1467

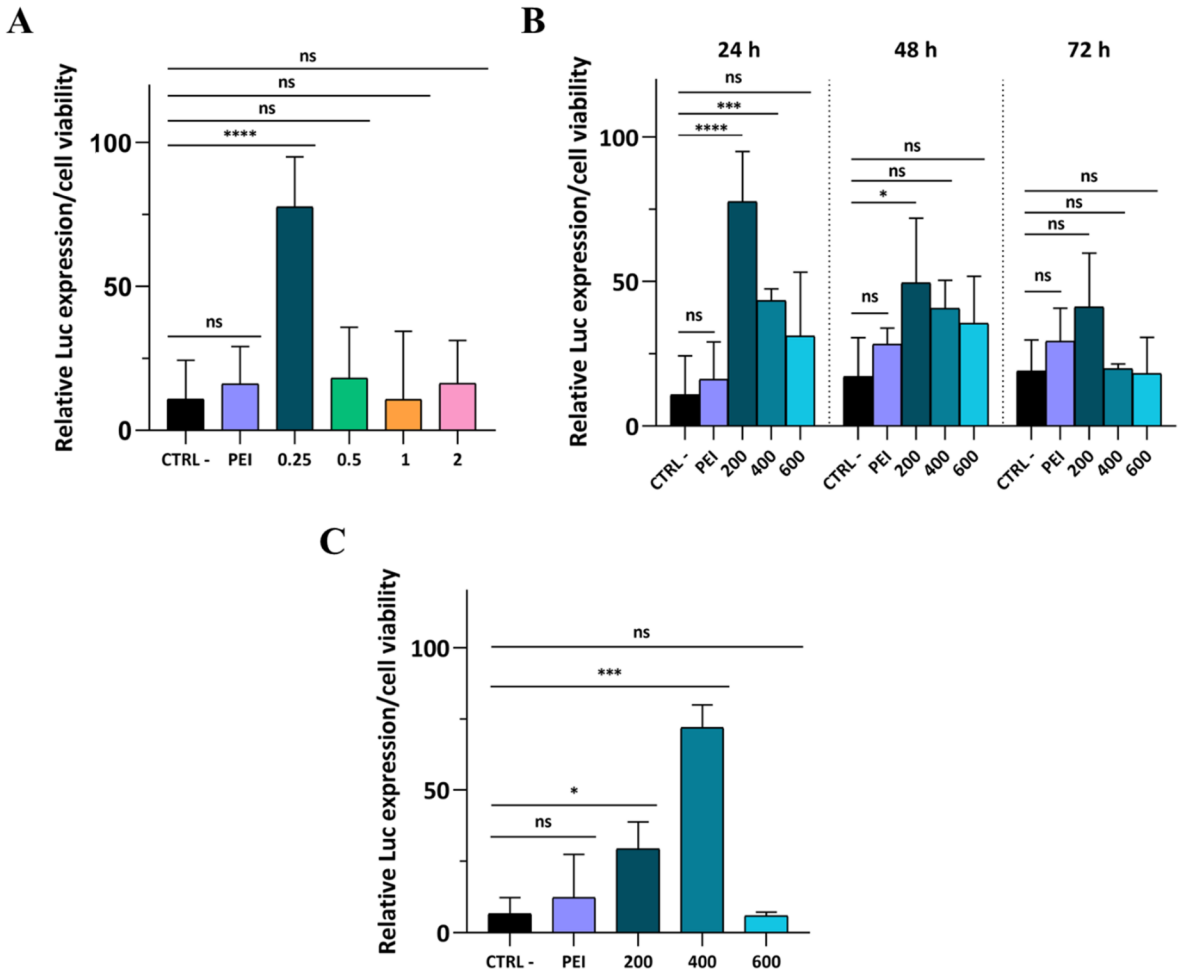

Figure 3. In vitro transfection of C-TRV3-A-px in 2D and 3D breast cancer cell culture models. A) In vitro transfection in 2D MDA-MB-231 cell cultures after a 24-h polyplex exposure (O/N ratio = 0.25, 0.5, 1, 2; N/*P* = 1). **B**) In vitro transfection in 2D MDA-MB-231 cell culture after a 24-, 48-, or 72-h Px02501 exposure at different pDNA-Luc concentrations (200, 400, 600 ng/mL). **C**) In vitro transfection in 3D MDA-MB-231 cell culture after a 24-h Px02501 exposure at different pDNA-Luc concentrations (200, 400, 600 ng/mL). Luciferase (Luc) activity quantified by measuring luminescence at 535 nm. Values normalized to cell viability and background subtracted. PEI (N/*P* = 1) used as a positive control and nonformulated pDNA-Luc used as a negative control (CTRL -). Values represent mean ± SEM ($n > 3$). Significance reported as p****<0.0001; p***<0.001; p**<0.01; p*<0.05; ns: not significant.

ization provides a promising platform for efficient and safe nonviral gene delivery, addressing the challenges of toxicity and stability associated with conventional polycationic systems.

3.4. Assessment of C-TRV3-A-Based Polyplex Stability and Hemocompatibility. Next, we conducted stability studies mimicking in vitro and in vivo conditions to assess the ability of C-TRV3-A-px to retain and release pDNA-Luc. We employed heparin displacement assays to assess C-TRV3-A-px stability and disassembly potential, leveraging the competing polyanion's ability to disrupt electrostatic interactions.[17,42]

Initially, we evaluated C-TRV3-A-px stability in DMEM + 10% FBS using shift-gel assays, as FBS contains abundant polyanionic molecules (including proteoglycans and glycosaminoglycans[43]) that may compete with polyplex components and facilitate oligonucleotide release. C-TRV3-A-px (O/P ratios = 0.25, 0.5, 1, and 2) demonstrated stability after 1-h incubation at 37 °C, while disassembly occurred upon the addition of excess heparin (50 IU/ml) (Figure 2D and S18).

To assess the potential for in vivo translation and intravenous administration, we determined the stability of Px02501 (O/P = 0.25, N/P = 1) in mouse and human plasma. Px02501 formulation remained stable after 1-h incubation at 37 °C in mouse plasma (Figure 2D and S19). Notably, Px02501 demonstrated stability in the presence of up to 0.75 IU/ml heparin, a value significantly higher than average heparin levels in human plasma (0.15 IU/ml)[44] (Figure S19). As expected, Px02501 disassembled in the presence of excess heparin (50 IU/ml) (Figure 2D and S19).

To validate the mouse model results, we also confirmed Px02501 stability in human plasma isolated from three healthy patients (Figure 2D and S20). Importantly, Px02501 disassembled in the presence of excess heparin (50 IU/ml) in human plasma (Figure 2D and S20). These results are particularly relevant considering that patient blood samples represented diverse physiological conditions. Variability in plasma components, such as proteins, lipoproteins, and coagulation factors, can influence protein corona formation, affecting polyplex stability.[45,46] The consistent stability of Px02501 in these samples suggests robustness in varying human plasma compositions, highlighting the potential of C-TRV3-A-px for clinical applications.

To evaluate hemocompatibility, we assessed the potential of Px02501 to induce the lysis of red blood cells. We conducted experiments at pH 7.4 to simulate conditions encountered in

https://doi.org/10.1021/acs.chemmater.4c02742
Chem. Mater. 2025, 37, 1457−1467

the bloodstream, extracellular space, and cytosol. We examined the hemolytic activity of Px02501 across a concentration range of 0.01−0.08 mg/mL (based on C-TRV3-A content). Results demonstrated a concentration-dependent hemolytic effect, with a maximum nonsignificant 20% of hemolysis (Figure S21). The observed low hemolytic activity suggests that Px02501 possesses favorable hemocompatibility characteristics, supporting its potential for future in vivo studies upon intravenous administration. Based on these findings, we established a maximum C-TRV3-A concentration of 0.08 mg/mL for subsequent activity experiments to ensure maintenance within safe hemolytic levels.

Our comprehensive stability and hemocompatibility studies demonstrate that C-TRV3-A-px exhibit robust stability under physiological conditions, controlled disassembly in the presence of competing polyanions, and favorable hemocompatibility, collectively supporting their potential for future in vivo gene delivery applications.

3.5. In Vitro Transfection of C-TRV3-A-Based Polyplexes in 2D and 3D Cell Models. After demonstrating the formation, stability, and hemocompatibility of C-TRV3-A-px, we aimed to verify their functionality as gene delivery vectors. To ensure the safety profile of C-TRV3-A-px under varying conditions (i.e., increased O/P ratio, extended incubation times, and higher doses), we evaluated cell viability for all experimental parameters, confirming their nontoxic nature throughout the study (Figures S22−24).

Initially, we tested the transfection efficiency of C-TRV3-A-px with different O/P ratios (0.25, 0.5, 1, and 2) in 2D MDA-MB-231 cell monolayers after 24 h, comparing them to nonformulated pDNA-Luc (negative control) and PEI at the same N/P ratio (=1). Our results demonstrated that Px02501 (O/P = 0.25, N/P = 1) exhibited the highest transfection efficiency, significantly outperforming other polyplexes and the positive control (Figure 3A). The significant performance compared to the gold standard PEI (typically evaluated at N/P ratio >4 in MDA-MB-231 cells[47]) at the same N/P ratio highlights the safer profile of C-TRV3-A-px due to the lower polycationic component concentration.

Next, we evaluated the transfection effectiveness of Px02501 as a function of the transfection time and plasmid dose. We observed the highest transfection efficiency for Px02501 at an incubation time of 24 h (Figure 3B). Transfection time inherently depends on the cell type to be transfected.[48] Interestingly, we observed a dose-independent transfection efficiency, with the highest Luc expression at the lowest plasmid concentration (200 ng/mL) compared to higher doses (400 and 600 ng/mL). Lower concentrations may provide an optimal balance between Px02501 formation and cellular uptake,[49] potentially avoiding aggregation[50,51] or saturation of internalization pathways at higher doses.[52]

Given the more realistic scenario offered by three-dimensional (3D) cell cultures such as spheroids in terms of cell−cell interactions and biochemical features[53−56] that may influence the in vitro efficiency of Px02501, we evaluated Luc transfection in MDA-MB-231 cell spheroids after 24 h. Our results demonstrate maintained transfection in 3D cell spheroids, with significant dose-dependent transfection (400 > 200 ng/mL) compared to 2D monolayer cell cultures, which decreased at the highest tested dose (Figure 3C). The differential behavior between 2D and 3D cell culture models underscores the importance of evaluating gene delivery systems in more physiologically relevant models.

These results demonstrate the efficacy of Px02501 as a gene delivery vector in both 2D and 3D cell culture models, highlighting their potential as safer and more efficient alternatives to conventional transfection agents.

4. CONCLUSIONS

We report the design, synthesis, and evaluation of a novel, versatile, and multifunctional polypeptide-based nanoconjugate (C-TRV3-A) for combined mitochondrial targeting and nonviral gene therapy. The rational chemical design, incorporating a PLO backbone, PEG modification, and a custom-designed trivalent compound (TRV3), enabled the creation of a versatile nanocarrier with controlled multifunctionality. The strategic inclusion of a redox-sensitive S−S linker and a TPP moiety facilitated TRV3 release and specific mitochondrial targeting of a model drug (Cy5). The modular synthetic approach allowed for precise control over the product's chemical identity and degree of functionalization through exhaustive physicochemical characterization steps, achieving a 3.6% mol PEG modification, 4% mol TRV3 conjugation, and less than 1 wt % fluorophore functionalization. The resulting nanoconjugate exhibited endosomal escape properties while retaining mitochondrial targeting capabilities. By incorporating an anionic polypeptide (VLC-3, $Psar_{100}$-*b*-PGA_{15}) shielding into the polyplex formation procedure, we further enhanced stability and transfection efficiency while mitigating toxicity concerns associated with polycationic polymers. In vitro evaluations in 2D and 3D cancer cell models revealed the superior performance of C-TRV3-A-px compared to conventional transfection agents. The observed structure−function relationships, particularly the impact of O/P and N/P ratios on polyplex stability and transfection efficiency, provide valuable insight for the rational design of future polypeptide-based delivery systems. This versatile platform opens new possibilities for tailored therapeutic approaches; future investigations should focus on in vivo validation, exploration of alternative payloads for mitochondrial-specific therapy, and the delivery of specific nucleic acid species (e.g., small interfering RNA) for cancer treatment.

■ ASSOCIATED CONTENT

Supporting Information

The Supporting Information is available free of charge at https://pubs.acs.org/doi/10.1021/acs.chemmater.4c02742.

Additional experimental details, including materials and general procedures, synthetic protocols, and characterization data for polypeptide-based nanoconjugates; analytical techniques such as NMR spectroscopy, mass spectrometry, dynamic light scattering, and transmission electron microscopy; small-angle X-ray scattering data and polyplex formation and characterization; biological studies, including cytotoxicity assays, cellular uptake studies, hemocompatibility tests, and transfection efficiency in 2D and 3D in vitro breast cancer models; statistical analysis; and references (PDF)

Video_S1_C-TRV3-A (MOV)

■ AUTHOR INFORMATION

Corresponding Authors

Inmaculada Conejos-Sanchez − *Príncipe Felipe Research Center, Polymer Therapeutics Lab., Valencia 46012, Spain; Centro de Investigación Biomédica en Red en Cáncer*

https://doi.org/10.1021/acs.chemmater.4c02742
Chem. Mater. 2025, 37, 1457−1467

(CIBERONC), Instituto de Salud Carlos III, Madrid 28029, Spain; orcid.org/0000-0002-4196-0855; Email: iconejos@cipf.es

María J. Vicent − *Príncipe Felipe Research Center, Screening Platform., Valencia 46012, Spain; Príncipe Felipe Research Center, Polymer Therapeutics Lab., Valencia 46012, Spain; Centro de Investigación Biomédica en Red en Cáncer (CIBERONC), Instituto de Salud Carlos III, Madrid 28029, Spain;* orcid.org/0000-0001-7771-3373; Email: mjvicent@cipf.es

Authors

Camilla Pegoraro − *Príncipe Felipe Research Center, Polymer Therapeutics Lab., Valencia 46012, Spain*

Esther Masiá Sanchis − *Príncipe Felipe Research Center, Polymer Therapeutics Lab., Valencia 46012, Spain; Centro de Investigación Biomédica en Red en Cáncer (CIBERONC), Instituto de Salud Carlos III, Madrid 28029, Spain; Príncipe Felipe Research Center, Screening Platform., Valencia 46012, Spain*

Snežana Đorđević − *Príncipe Felipe Research Center, Polymer Therapeutics Lab., Valencia 46012, Spain; Centro de Investigación Biomédica en Red en Cáncer (CIBERONC), Instituto de Salud Carlos III, Madrid 28029, Spain;* Present Address: S.D.: Tosoh Bioscience, Im Leuschnerpark 4, 64347 Griesheim, Germany; orcid.org/0000-0001-8429-7486

Irene Dolz-Pérez − *Curapath, Paterna, Valencia 46980, Spain;* orcid.org/0000-0002-0447-0718

Cristián Huck-Iriart − *Experiments Division, ALBA Synchrotron Light Source, Cerdanyola del Vallès 08209, Spain;* orcid.org/0000-0001-5734-2499

Lidia Herrera − *Curapath, Paterna, Valencia 46980, Spain*

Sergio Esteban-Pérez − *Curapath, Paterna, Valencia 46980, Spain*

Complete contact information is available at: https://pubs.acs.org/10.1021/acs.chemmater.4c02742

Author Contributions

C.P., I.C.-S., and M.J.V. developed the concept and design of the project. Synthesis and physicochemical characterization of the nanoconjugates were performed by C.P. and SD. Synthesis of VLC-3 L.H. Polyplex formation and stability studies were carried out by C.P. and I.C.-S, with protocols optimized by I.D.-P. and S.E.-P. for VLC-3 use. SAXS analysis was carried out by C.H.-I. In vitro setup studies were performed by C.P. and E.M. Gene transfection studies were performed by C.P. Analysis and interpretation of the data included the contribution of all authors. M.J.V. was responsible for funding acquisition and supervision together with I.C.-S. The manuscript was written and edited by C.P., I.C.-S., and M.J.V. and was revised by the rest of the authors. All authors have read and approved the final version of the manuscript.

Funding

This project was supported by the H2020-MSCA-ITN-2019 BIOMOLMACS (Grant Agreement No. 859416). The authors gratefully acknowledge financial support from the Asociación Española contra el Cáncer (ICS INVES211323CONE, Junior AECC grant), the Ministerio de Ciencia, Tecnología e Innovación (Grants PID2019−108806RB-100 and PID2023−152459OB-I00), and NextGeneration EU i+D+I funding through the GVA Conselleria de Innovación − Pol@ Mets (ref. MFA/2022/065). Additionally, support from the European Regional Development Fund (PO FEDER Comunitat Valenciana 2014−2020), Generalitat Valenciana, is acknowledged. Small-angle X-ray scattering (SAXS) measurements were conducted at the NCD-SWEET beamline of the ALBA Synchrotron Light Source (Barcelona, Spain) under Project ID 2022097124. Furthermore, we acknowledge support from the Horizon Europe EU-OPENSCREEN IMPULSE project (Grant Agreement No. 101132028).

Notes

The authors declare the following competing financial interest(s): Sergio Esteban-Perez and Lidia Herrero from Curapath are co-inventors of the patent covering the rights of VLC3.

■ ACKNOWLEDGMENTS

We thank Dr. Stuart P. Atkinson for his help in manuscript development and English editing, Alberto Hernández for confocal imaging support, and Mario Soriano for TEM support. We thank the student Kato D'Huawe from Ghent University for her help in the experimental work.

■ REFERENCES

(1) Shi, J.; Kantoff, P. W.; Wooster, R.; Farokhzad, O. C. Cancer Nanomedicine: Progress, Challenges and Opportunities. *Nat. Rev. Cancer* **2017**, *17* (1), 20−37.

(2) Gao, Y.; Wang, K.; Zhang, J.; Duan, X.; Sun, Q.; Men, K. *Multifunctional Nanoparticle for Cancer Therapy. MedComm* **2023**, *4* (1), No. e187.

(3) Chen, W.-H.; Luo, G.-F.; Zhang, X.-Z. Recent Advances in Subcellular Targeted Cancer Therapy Based on Functional Materials. *Adv. Mater.* **2019**, *31* (3), 1802725.

(4) Zagorodko, O.; Arroyo-Crespo, J. J.; Nebot, V. J.; Vicent, M. J. Polypeptide-Based Conjugates as Therapeutics: Opportunities and Challenges. *Macromol. Biosci.* **2017**, *17* (1), 1600316.

(5) Duro-Castano, A.; Conejos-Sánchez, I.; Vicent, M. J. Peptide-Based Polymer Therapeutics. *Polymers.* **2014**, *6*, 515−551.

(6) Melnyk, T.; Đorđević, S.; Conejos-Sánchez, I.; Vicent, M. J. Therapeutic Potential of Polypeptide-Based Conjugates: Rational Design and Analytical Tools That Can Boost Clinical Translation. *Adv. Drug Delivery Rev.* **2020**, *160*, 136−169.

(7) Galic, V. L.; Wright, J. D.; Lewin, S. N.; Herzog, T. J. Paclitaxel Poliglumex for Ovarian Cancer. *Expert Opin. Investig. Drugs* **2011**, *20* (6), 813−821.

(8) Wang, X.; Song, Z.; Wei, S.; Ji, G.; Zheng, X.; Fu, Z.; Cheng, J. Polypeptide-Based Drug Delivery Systems for Programmed Release. *Biomaterials* **2021**, *275*, No. 120913.

(9) Li, X.; Liu, J.; Chen, H.; Chen, Y.; Wang, Y.; Zhang, C. Y.; Xing, X.-H. Multi-Functional Engineered Polypeptide-Based Drug Delivery Systems for Improved Cancer Therapy. *Green Chem. Eng.* **2023**, *4* (2), 173−188.

(10) Liu, Y.; Yin, L. α-Amino Acid N-Carboxyanhydride (NCA)-Derived Synthetic Polypeptides for Nucleic Acids Delivery. *Adv. Drug Delivery Rev.* **2021**, *171*, 139−163.

(11) Zhao, B.; Zhang, X.; Bickle, M. S.; Fu, S.; Li, Q.; Zhang, F. Development of Polypeptide-Based Materials toward Messenger RNA Delivery. *Nanoscale* **2024**, *16* (5), 2250−2264.

(12) Pegoraro, C.; Karpova, E.; Qutbuddin, Y.; Sanchis, E. M.; Dimitrijevs, P.; Huck-Iriart, C.; Gavrilović, S.; Arsenyan, P.; Schwille, P.; Felip-León, C.; Duro-Castano, A.; Conejos-Sanchez, I.; Vicent, M. J. Polyproline-polyornithine diblock copolymers with inherent mitochondria tropism. *Adv. Mater.* **2025**, 2411595.

(13) Cohen-Erez, I.; Rapaport, H. Coassemblies of the Anionic Polypeptide γ-PGA and Cationic β-Sheet Peptides for Drug Delivery to Mitochondria. *Biomacromolecules* **2015**, *16* (12), 3827−3835.

(14) Porporato, P. E.; Filigheddu, N.; Pedro, J. M. B.-S.; Kroemer, G.; Galluzzi, L. Mitochondrial Metabolism and Cancer. *Cell Res.* **2018**, *28* (3), 265−280.
(15) Pegoraro, C.; Domingo-Ortí, I.; Conejos-Sánchez, I.; Vicent, M. J. Unlocking the Mitochondria for Nanomedicine-Based Treatments: Overcoming Biological Barriers, Improving Designs, and Selecting Verification Techniques. *Adv. Drug Delivery Rev.* **2024**, *207*, No. 115195.
(16) Suk, J. S.; Xu, Q.; Kim, N.; Hanes, J.; Ensign, L. M. PEGylation as a Strategy for Improving Nanoparticle-Based Drug and Gene Delivery. *Adv. Drug Delivery Rev.* **2016**, *99*, 28−51.
(17) Conejos-Sánchez, I.; Gallon, E.; Niño-Pariente, A.; Smith, J. A.; De la Fuente, A. G.; Di Canio, L.; Pluchino, S.; Franklin, R. J. M.; Vicent, M. J. Polyornithine-Based Polyplexes to Boost Effective Gene Silencing in CNS Disorders. *Nanoscale* **2020**, *12* (11), 6285−6299.
(18) Cheng, X.; Feng, D.; Lv, J.; Cui, X.; Wang, Y.; Wang, Q.; Zhang, L. Application Prospects of Triphenylphosphine-Based Mitochondria-Targeted Cancer Therapy. *Cancers.* **2023**, *15*, 666.
(19) Zielonka, J.; Joseph, J.; Sikora, A.; Hardy, M.; Ouari, O.; Vasquez-Vivar, J.; Cheng, G.; Lopez, M.; Kalyanaraman, B. Mitochondria-Targeted Triphenylphosphonium-Based Compounds: Syntheses, Mechanisms of Action, and Therapeutic and Diagnostic Applications. *Chem. Rev.* **2017**, *117* (15), 10043−10120.
(20) Fu, S.; Rempson, C. M.; Puche, V.; Zhao, B.; Zhang, F. Construction of Disulfide Containing Redox-Responsive Polymeric Nanomedicine. *Methods* **2022**, *199*, 67−79.
(21) Saviano, F.; Lovato, T.; Russo, A.; Russo, G.; Bouton, C. R.; Shattock, R. J.; Alexander, C.; Quaglia, F.; Blakney, A. K.; Gurnani, P.; Conte, C. Ornithine-Derived Oligomers and Dendrimers for in Vitro Delivery of DNA and Ex Vivo Transfection of Skin Cells via SaRNA. *J. Mater. Chem. B* **2020**, *8* (22), 4940−4949.
(22) Ramsay, E.; Gumbleton, M. Polylysine and Polyornithine Gene Transfer Complexes: A Study of Complex Stability and Cellular Uptake as a Basis for Their Differential in-Vitro Transfection Efficiency. *J. Drug Target.* **2002**, *10* (1), 1−9.
(23) Ramsay, E.; Hadgraft, J.; Birchall, J.; Gumbleton, M. Examination of the Biophysical Interaction between Plasmid DNA and the Polycations, Polylysine and Polyornithine, as a Basis for Their Differential Gene Transfection in-Vitro. *Int. J. Pharm.* **2000**, *210* (1), 97−107.
(24) Barrett, S. E.; Burke, R. S.; Abrams, M. T.; Bason, C.; Busuek, M.; Carlini, E.; Carr, B. A.; Crocker, L. S.; Fan, H.; Garbaccio, R. M.; Guidry, E. N.; Heo, J. H.; Howell, B. J.; Kemp, E. A.; Kowtoniuk, R. A.; Latham, A. H.; Leone, A. M.; Lyman, M.; Parmar, R. G.; Patel, M.; Pechenov, S. Y.; Pei, T.; Pudvah, N. T.; Raab, C.; Riley, S.; Sepp-Lorenzino, L.; Smith, S.; Soli, E. D.; Staskiewicz, S.; Stern, M.; Truong, Q.; Vavrek, M.; Waldman, J. H.; Walsh, E. S.; Williams, J. M.; Young, S.; Colletti, S. L. Development of a Liver-Targeted SiRNA Delivery Platform with a Broad Therapeutic Window Utilizing Biodegradable Polypeptide-Based Polymer Conjugates. *J. Controlled Release* **2014**, *183*, 124−137.
(25) Lv, H.; Zhang, S.; Wang, B.; Cui, S.; Yan, J. Toxicity of Cationic Lipids and Cationic Polymers in Gene Delivery. *J. Controlled Release* **2006**, *114* (1), 100−109.
(26) Zhao, X.; Li, X.; Zhao, Y.; Cheng, Y.; Yang, Y.; Fang, Z.; Xie, Y.; Liu, Y.; Chen, Y.; Ouyang, Y.; Yuan, W. Immune Activities of Polycationic Vectors for Gene Delivery. *Front. Pharmacol.* **2017**, *8*, 510−517.
(27) Wang, Y.; Ye, M.; Xie, R.; Gong, S. Enhancing the In Vitro and In Vivo Stabilities of Polymeric Nucleic Acid Delivery Nanosystems. *Bioconjugate Chem.* **2019**, *30* (2), 325−337.
(28) Felip, C.; Dolz, I.; Esteban-Pérez, S.; Herrera-Muñoz, L. N.-C. V.Non-Covalent Shielding Polymers. WO2023002014A1. WO EP CN JP CA. Prior. *2021−07−22, Filed 2022−07−22, Publ. 2023−01−26*.
(29) Sing, C. E. Development of the Modern Theory of Polymeric Complex Coacervation. *Adv. Colloid Interface Sci.* **2017**, *239*, 2−16.
(30) Behzadi, S.; Serpooshan, V.; Tao, W.; Hamaly, M. A.; Alkawareek, M. Y.; Dreaden, E. C.; Brown, D.; Alkilany, A. M.; Farokhzad, O. C.; Mahmoudi, M. Cellular Uptake of Nanoparticles: Journey inside the Cell. *Chem. Soc. Rev.* **2017**, *46* (14), 4218−4244.
(31) Hammouda, B. Small-Angle Scattering From Branched Polymers. *Macromol. Theory Simulations* **2012**, *21* (6), 372−381.
(32) Borchert, H.; Shevchenko, E. V.; Robert, A.; Mekis, I.; Kornowski, A.; Grübel, G.; Weller, H. Determination of Nanocrystal Sizes: A Comparison of TEM, SAXS, and XRD Studies of Highly Monodisperse CoPt3 Particles. *Langmuir* **2005**, *21* (5), 1931−1936.
(33) Brülisauer, L.; Gauthier, M. A.; Leroux, J.-C. Disulfide-Containing Parenteral Delivery Systems and Their Redox-Biological Fate. *J. Controlled Release* **2014**, *195*, 147−154.
(34) Kennedy, L.; Sandhu, J. K.; Harper, M.-E.; Cuperlovic-Culf, M. Role of Glutathione in Cancer: From Mechanisms to Therapies. *Biomolecules.* **2020**, *10*, 1429.
(35) Tros de Ilarduya, C.; Sun, Y.; Düzgüneş, N. Gene Delivery by Lipoplexes and Polyplexes. *Eur. J. Pharm. Sci.* **2010**, *40* (3), 159−170.
(36) Dirisala, A.; Uchida, S.; Li, J.; Van Guyse, J. F. R.; Hayashi, K.; Vummaleti, S. V. C.; Kaur, S.; Mochida, Y.; Fukushima, S.; Kataoka, K. Effective MRNA Protection by Poly(l-Ornithine) Synergizes with Endosomal Escape Functionality of a Charge-Conversion Polymer toward Maximizing MRNA Introduction Efficiency. *Macromol. Rapid Commun.* **2022**, *43* (12), 2100754.
(37) Cai, M.; Zhang, Z.; Su, X.; Dong, H.; Zhong, Z.; Zhuo, R. Guanidinated Multi-Arm Star Polyornithines with a Polyethylenimine Core for Gene Delivery. *Polymer (Guildf).* **2014**, *55* (18), 4634−4640.
(38) Koloskova, O. O.; Nikonova, A. A.; Budanova, U. A.; Shilovskiy, I. P.; Kofiadi, I. A.; Ivanov, A. V.; Smirnova, O. A.; Zverev, V. V.; Sebaykin, Y. L.; Andreev, S. M.; Khaitov, M. R. Synthesis and Evaluation of Novel Lipopeptide as a Vehicle for Efficient Gene Delivery and Gene Silencing. *Eur. J. Pharm. Biopharm.* **2016**, *102*, 159−167.
(39) Ito, T.; Iida-Tanaka, N.; Niidome, T.; Kawano, T.; Kubo, K.; Yoshikawa, K.; Sato, T.; Yang, Z.; Koyama, Y. Hyaluronic Acid and Its Derivative as a Multi-Functional Gene Expression Enhancer: Protection from Non-Specific Interactions, Adhesion to Targeted Cells, and Transcriptional Activation. *J. Controlled Release* **2006**, *112* (3), 382−388.
(40) Tian, H.; Lin, L.; Chen, J.; Chen, X.; Park, T. G.; Maruyama, A. RGD Targeting Hyaluronic Acid Coating System for PEI-PBLG Polycation Gene Carriers. *J. Controlled Release* **2011**, *155* (1), 47−53.
(41) He, Y.; Cheng, G.; Xie, L.; Nie, Y.; He, B.; Gu, Z. Polyethyleneimine/DNA Polyplexes with Reduction-Sensitive Hyaluronic Acid Derivatives Shielding for Targeted Gene Delivery. *Biomaterials* **2013**, *34* (4), 1235−1245.
(42) Zhang, H.; Gao, X.; Sun, Q.; Dong, X.; Zhu, Z.; Yang, C. Incorporation of Poly(γ-Glutamic Acid) in Lipid Nanoparticles for Enhanced MRNA Delivery Efficiency in Vitro and in Vivo. *Acta Biomater.* **2024**, *177*, 361−376.
(43) Pérez-Rubio, P.; Vendrell-Flotats, M.; Romero, E. L.; Enemark-Rasmussen, K.; Cervera, L.; Gòdia, F.; Lavado-García, J. Internalization of PEI-Based Complexes in Transient Transfection of HEK293 Cells Is Triggered by Coalescence of Membrane Heparan Sulfate Proteoglycans like Glypican-4. *Biomed. Pharmacother.* **2024**, *176*, No. 116893.
(44) ENGELBERG, H. Plasma Heparin Levels. Correlation with Serum Cholesterol and Low-Density Lipoproteins. *Circulation* **1961**, *23* (April), 573−577.
(45) Hartl, N.; Jürgens, D. C.; Carneiro, S.; König, A.-C.; Xiao, X.; Liu, R.; Hauck, S. M.; Merkel, O. M. Protein Corona Investigations of Polyplexes with Varying Hydrophobicity − From Method Development to in Vitro Studies. *Int. J. Pharm.* **2023**, *643*, No. 123257.
(46) Zhu, D.; Yan, H.; Zhou, Z.; Tang, J.; Liu, X.; Hartmann, R.; Parak, W. J.; Shen, Y.; Feliu, N. Influence of the Modulation of the Protein Corona on Gene Expression Using Polyethylenimine (PEI) Polyplexes as Delivery Vehicle. *Adv. Healthc. Mater.* **2021**, *10* (13), 2100125.
(47) Zhang, H.; Chen, Z.; Du, M.; Li, Y.; Chen, Y. Enhanced Gene Transfection Efficiency by Low-Dose 25 KDa Polyethylenimine by

the Assistance of 1.8 KDa Polyethylenimine. *Drug Delivery* **2018**, *25* (1), 1740−1745.
(48) Malloggi, C.; Pezzoli, D.; Magagnin, L.; De Nardo, L.; Mantovani, D.; Tallarita, E.; Candiani, G. Comparative Evaluation and Optimization of Off-the-Shelf Cationic Polymers for Gene Delivery Purposes. *Polym. Chem.* **2015**, *6* (35), 6325−6339.
(49) Zhang, Z.; Qiu, N.; Wu, S.; Liu, X.; Zhou, Z.; Tang, J.; Liu, Y.; Zhou, R.; Shen, Y. Dose-Independent Transfection of Hydrophobized Polyplexes. *Adv. Mater.* **2021**, *33* (25), 2102219.
(50) Pezzoli, D.; Giupponi, E.; Mantovani, D.; Candiani, G. Size Matters for in Vitro Gene Delivery: Investigating the Relationships among Complexation Protocol, Transfection Medium, Size and Sedimentation. *Sci. Rep.* **2017**, *7* (1), 44134.
(51) D'Andrea, C.; Pezzoli, D.; Malloggi, C.; Candeo, A.; Capelli, G.; Bassi, A.; Volonterio, A.; Taroni, P.; Candiani, G. The Study of Polyplex Formation and Stability by Time-Resolved Fluorescence Spectroscopy of SYBR Green I-Stained DNA. *Photochem. Photobiol. Sci.* **2014**, *13* (12), 1680−1689.
(52) Monnery, B. D. Polycation-Mediated Transfection: Mechanisms of Internalization and Intracellular Trafficking. *Biomacromolecules* **2021**, *22* (10), 4060−4083.
(53) Boix-Montesinos, P.; Soriano-Teruel, P. M.; Armiñán, A.; Orzáez, M.; Vicent, M. J. The Past, Present, and Future of Breast Cancer Models for Nanomedicine Development. *Adv. Drug Delivery Rev.* **2021**, *173*, 306−330.
(54) Satchi-Fainaro, R.; Florindo, H. F.; Vicent, M. J. Clinically-Relevant and Predictive Cancer Models for Nanomedicine Evaluation. *Adv. Drug Delivery Rev.* **2022**, *183*, No. 114140.
(55) Monfared, Y. K.; Mahmoudian, M.; Cecone, C.; Caldera, F.; Haiaty, S.; Heidari, H. R.; Rahbarghazi, R.; Matencio, A.; Zakeri-Milani, P.; Trotta, F. Hyper-Branched Cationic Cyclodextrin Polymers for Improving Plasmid Transfection in 2D and 3D Spheroid Cells. *Pharmaceutics.* **2022**, *14*, 2690.
(56) Pinto, B.; Henriques, A. C.; Silva, P. M. A.; Bousbaa, H. Three-Dimensional Spheroids as In Vitro Preclinical Models for Cancer Research. *Pharmaceutics.* **2020**, *12*, 1186.

https://doi.org/10.1021/acs.chemmater.4c02742
Chem. Mater. 2025, 37, 1457−1467